Int J Adv Manuf Technol (2017) 90:291–298
DOI 10.1007/s00170-016-9365-y

ORIGINAL ARTICLE

Structural and martensitic transformation of MnNiSn shape memory alloys

H. Rekik[1] · **M. Krifa**[1] · **T. Bachaga**[1,2] · **L. Escoda**[1,2] · **J. J. Sunol**[2] · **M. Khitouni**[1] · **M. Chmingui**[1]

Received: 8 March 2016 / Accepted: 19 August 2016 /

Abstract Ferromagnetic shape memory alloys are characterized by both the structural austenite to martensite transformation and also by the magnetic transition from ferromagnetic to paramagnetic. The set of properties makes them candidates for use in several applications such as sensors, actuators, or magnetic refrigeration systems. Among the Heusler-type alloys that exhibit this behavior, the most studied system is the Ni–Mn–Ga. However, to overcome the high cost of Gallium and the generally low martensitic transformation temperature, the search for Ga-free alloys has been recently attempted, particularly, by introducing Sn. The martensitic transformation and the solidification structures of $Mn_{50}Ni_{50-x}Sn_x$ ($x = 7$, 8.7 and 10.5) ribbons prepared by melt-spinning were investigated by means of scanning electron microscopy, X-ray diffraction, and differential scanning calorimetry. While the As-spun alloys $Mn_{50}Ni_{43}Sn_7$ and $Mn_{50}Ni_{41.3}Sn_{8.7}$ displayed a single-phase (14-M monoclinic martensite) structure at room temperature, the As-spun and $Mn_{50}Ni_{39.5}Sn_{10.5}$ displayed a single-phase cubic Heusler $L2_1$. The martensitic transformation temperatures were noted to decrease with the increase of Sn concentration.

Keywords Heusler alloys · Martensitic transition · Thermal analysis · X-ray diffraction · Rapid solidification

1 Introduction

Heusler-based ferromagnetic shape memory alloys Mn–Ni–Z (Z = In, Sn, Sb) have received increasing attention due to their ability to undergo a reversible first-order martensitic transformation (FOMT) from a high-temperature cubic austenite phase to a structurally modulated martensitic phase [1–3], the structure of which can be 10 M, 14 M, and $L1_0$ depending on the composition and manufacturing conditions.

Melt-spinning technology is an efficient and fast preparation technique of polycrystalline ribbons. It is capable of producing materials with a high degree of structural uniformity and fine grain structure [4, 5]. The rapid solidification of alloys by the melt-spinning process can lead to better mechanical properties compared to those obtainable by conventional casting [6].

In addition, rapid solidification from the liquid phase can result in atoms being located in a non-equilibrium state. This allows for a modification of the atomic order, and thus it is of great interest to investigate melt-spun ribbon materials. Recently, some interesting reports on the physical properties of Ni–Mn–X alloy ribbons have been published. Hernando et al. [7, 8] found that the crystal structure of martensite phase formed in Ni–Mn–X ribbons is different from that of bulk arc-melted materials.

In ternary Ni–Mn–X (X = In, Sn, Sb) FSMAs, the MT temperatures can be tuned by alloy composition, preparation condition, and external parameters (magnetic field and hydrostatic pressure [9]). Several factors have been proposed to affect the value of MT temperatures. MT temperatures can be tuned by changing the valence electron concentration (*e/a*) through composition variation or 3D transition metal substitution such as Cr, Fe, Co, and Cu [10–13]. The

---

✉ M. Khitouni
khitouni@yahoo.fr

[1] Laboratoire de Chimie Inorganique, UR-11-ES-73, Université de Sfax, B. P. 1171, 3000 Sfax, Tunisia

[2] Departamento de Fisica, Universitat de Girona, Campus Montilivi, 17071 Girona, Spain

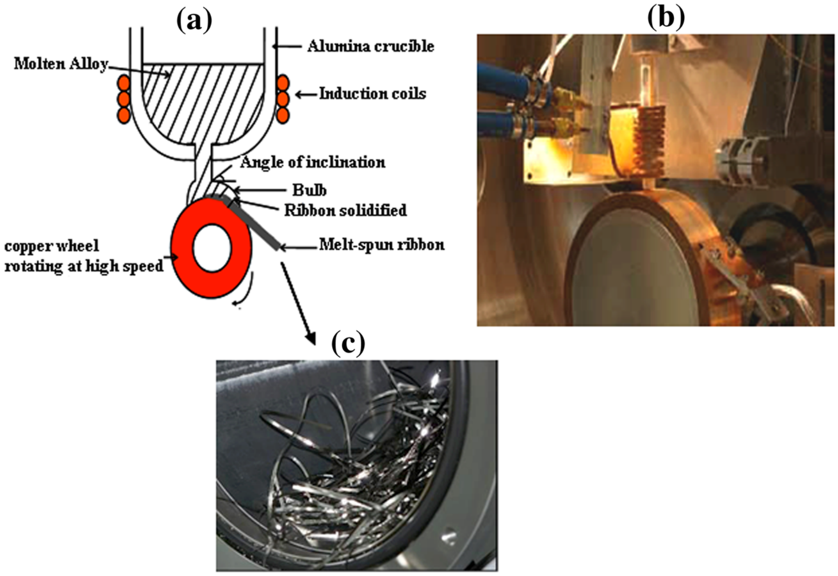

Fig. 1 Melt-spinning technique mechanism

compositional dependence of the phase-transition temperature is also attributed to the change in electron concentration and the Mn–Mn interatomic distance [14, 15].

Now, most FSMAs are Ni–Mn-based and can be obtained by the substitution of some main group elements (Ga for example) for Mn or Ni in NiMn alloys [16]. This substitution

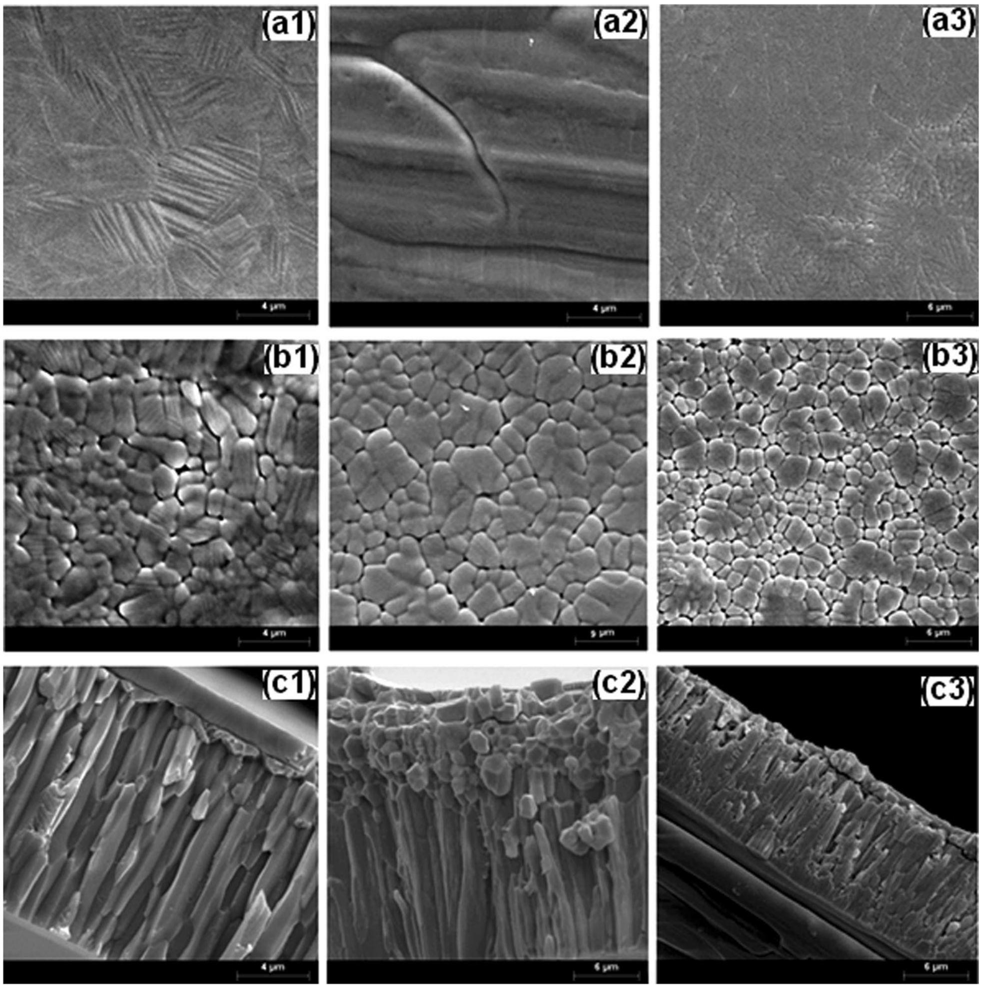

Fig. 2 Typical SEM micrographs of the different regions: (**a1**, **a2**, **a3**) the wheel surfaces, (**b1**, **b2**, **b3**) the free surfaces, and (**c1**, **c2**, **c3**) the cross-section microstructure of the As-spun ribbons $Mn_{50}Ni_{43}Sn_7$, $Mn_{50}Ni_{41.3}Sn_{8.7}$ and $Mn_{50}Ni_{39.5}Sn_{10.5}$, respectively

lowers the martensitic transformation temperature of NiMn effectively and results in a highly ordered Heusler-type structure. This makes it possible to predict the martensite transformation by first-principle calculations in Ni–Mn-based Heusler alloys. Further, Bachaga et al. [17] reported that melt-spinning processing parameters such as the linear surface speed of the copper wheel rotating, the injection overpressure, and the distance between wheel and injection quartz tube influence the microstructure of ribbons. In fact, transformation entropy was found higher when increasing linear surface speed or the distance from injection point to wheel. Also, a strong dependence of ribbon thickness on processing parameters was found. The average grain size varied between 1.6 and 6.6 μm, while the start temperature of the martensitic temperature varied from 394 to 430 K.

In this paper, we report the structural properties of $Mn_{50}Ni_{40-x}Sn_x$(x = 7, 8.7 and 10.5) Heusler alloys. The change in Sn concentration was found to affect the martensitic transition temperatures of these alloys.

2 Experimental procedure

As-cast ingots with a nominal composition of $Mn_{50}Ni_{50-x}Sn_x$ (x = 7, 8.7 and 10.5) were labeled as Sn7, Sn8.7, and Sn10.7, respectively. The ingots were prepared by arc-melting technique in argon atmosphere from high purity (99.99 %) elemental metals, using Bühler MAM-1 compact arc melting. These alloys were melted four times to ensure a good starting homogeneity. The samples were induction melted in quartz crucibles with a circular nozzle of 0.5 mm and ejected applying an argon overpressure on the polished surface of copper wheel rotating at a linear speed of 48 ms^{-1} (see Fig. 1a–b). The obtained As-quenched ribbons were flakes of 1.2–2.0 mm in width and 4–12 mm in length (see Fig. 1c).

Thermal and structural analyses were performed by applying several techniques: The microstructure and elemental compositions were examined by using a scanning electron microscope (SEM) equipped with an X-ray energy dispersive spectroscopy (EDS) microanalysis system. The structural characterization of the samples was performed at room temperature (RT) by X-ray diffractograms (XRD), using a Siemens D500 X-ray powder diffractometer with Cu-Kα radiation (λ = 1.5418 Å). The structures of the samples were refined using Maud program [18].

The austenite–martensite structural transformation was checked by calorimetry. The cyclic experiments (heating–cooling) were recorded at 10 K/min under Argon atmosphere. DSC scans above room temperature were performed in the DSC modulus of the Setaram Setsys system. The DSC measurements were carried out to examine the characteristic temperatures of MT, and the phase-transition activation energy was calculated on the basis of the DSC measurements.

3 Results and discussion

The typical SEM images of the wheel surfaces of alloys with Sn7, Sn8.7, and Sn10.5 are presented in Fig. 2a1, a2, and a3, respectively. The wheel surfaces of the Sn7 and Sn8.7 ribbons clearly present the lamellar microstructure of the martensite structure (Fig. 2a1, a2). While the wheel surface of the Sn10.5 ribbons is characterized by a granular microstructure of the austenite structure (Fig. 2a3). These ribbons are mechanically fragile and brittle and cleave easily along this normal direction.

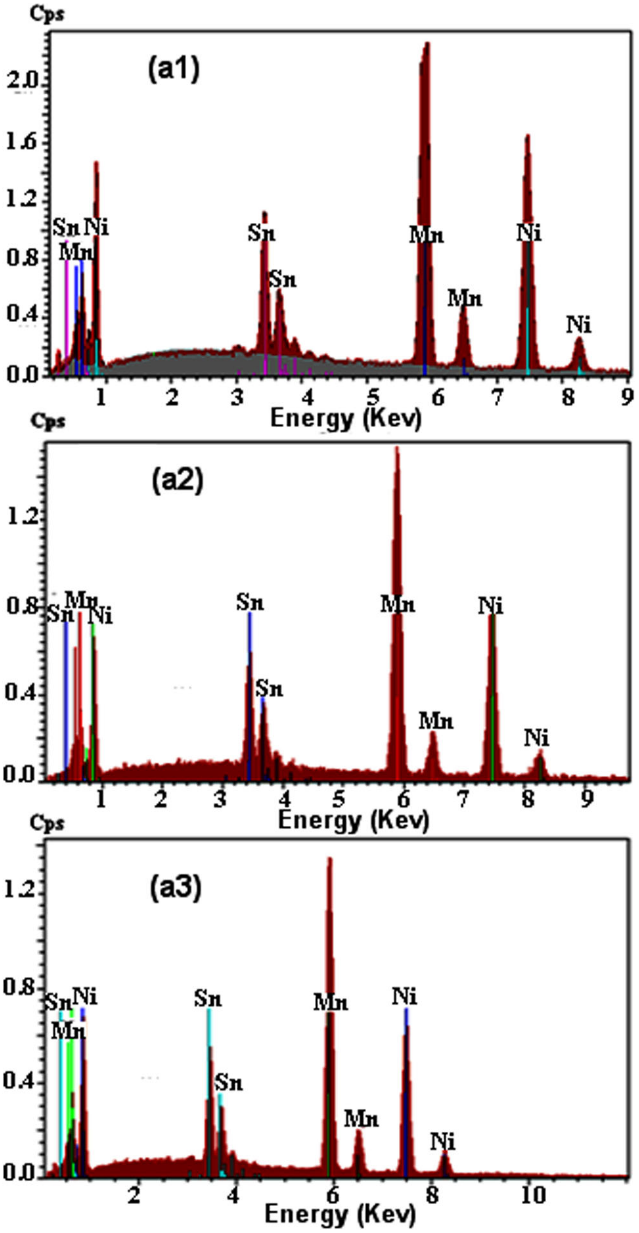

Fig. 3 ED's analysis of the As-spun ribbons $Mn_{50}Ni_{43}Sn_7$, $Mn_{50}Ni_{41.3}Sn_{8.7}$ and $Mn_{50}Ni_{39.5}Sn_{10.5}$ ribbons, respectively

Fig. 4 X-ray diffraction pattern at room temperature for (**a**) $Mn_{50}Ni_{43}Sn_7$, (**b**) $Mn_{50}Ni_{41.3}Sn_{8.7}$, and (**c**) $Mn_{50}Ni_{39.5}Sn_{10.5}$ samples, respectively

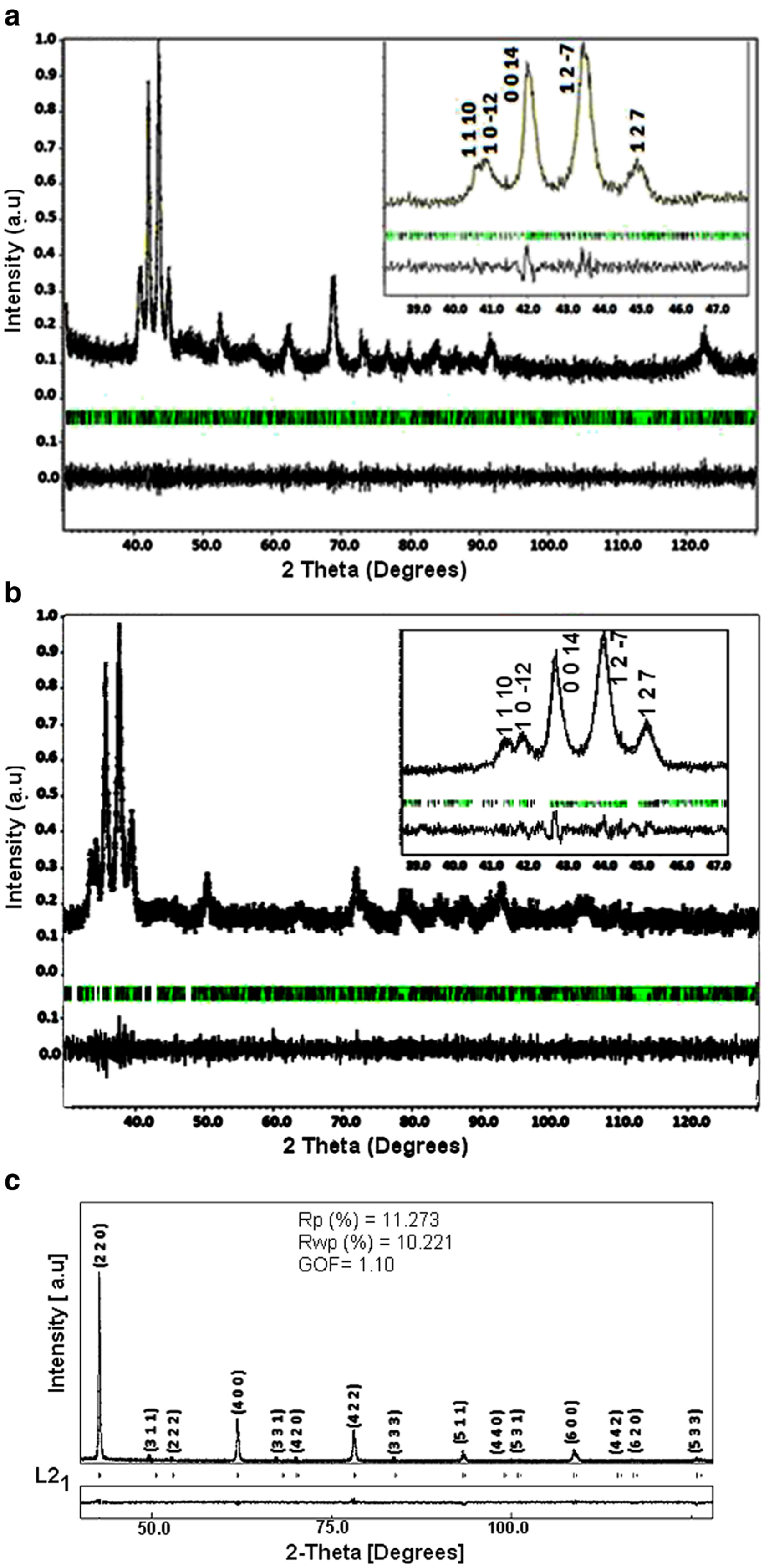

Table 1 Crystallographic parameters of $Mn_{50}Ni_{50-x}Sn_x$ ($x = 7$, 8.7 and 10.5) alloys

Alloys	Crystalline structure	Lattice parameters (nm)
Sn7	Monoclinic 14 M	$a = 0.4301$ $b = 0.5610$ $c = 2.9967$ $\beta = 93.37°$
Sn8.7	Monoclinic 14 M	$a = 0.4315$ $b = 0.5797$ $c = 3.0245$ $\beta = 93.84°$
Sn10.5	Cubic $L2_1$	$a = 0.599$

The free surfaces of alloys Sn7, Sn8.7, and Sn10.5 are presented in Fig. 2b1, b2, and b3; these samples obtained at high-quenching rates were fully crystalline and with a granular microstructure. The average grain size value was around 1–2 μm. Ribbons are mechanically fragile and brittle, and cleave easily along this normal direction. Further, average grain size values are well below the obtained value in bulk alloys exhibiting coarse grained microstructures with grain sizes varying from 10 to 100 μm [2].

The cross-sections for Sn7, Sn8.7, and Sn10.5 alloys normal to ribbon planes can be observed in Figs. 2c1 and 1c2 and c3, respectively. They demonstrate that the samples were fully crystalline, and their fracture surfaces revealed a fast crystallization and growth kinetics of the alloy. It also showed a collinear granular columnar type microstructure (Fig. 2c1–c3). The Sn7, Sn8.7, and Sn10.5 ribbon thickness were around 10, 15, and 8 μm, respectively. The thin layer of small equiaxed grains crystallized through the whole ribbon thickness, with the longest axis being aligned perpendicular to the ribbon plane.

Some EDX measurements were performed on each ribbon surface in order to check the homogeneity of the final composition. The EDX analysis of the As-spun ribbons is shown in Fig. 3a1, a2, and a3. The results confirm the presence of the mixed metallic elements. The composition analysis was found to be in good agreement with the nominal compositions of the As-spun ribbons ((49.7 at.% Mn-43.5 at.% Ni-6.8 at.% Sn), (50.3 at.% Mn-41.2 at.% Ni-8.5 at.% Sn) and (50.2 at.% Ni-39.5 at.% Mn-10.3 at.% Sn)). Compositions are shifted from the original. It is habitual in these alloys obtained by a two-step procedure: arc melting and melt spinning.

The knowledge of the crystal structure at room temperature is often essential to determine thermal analysis conditions [19]. If a cubic phase is detected, the martensite–austenite transition must be below room temperature. If, on the other hand, the phase is orthorhombic, monoclinic, or tetragonal, the same transition could be obtained by heating the alloy at room temperature. Figure 4 (a, b, c) shows the XRD patterns 172 of Sn7, Sn8.7, and Sn10.5 ribbons analyzed at room temperature. Miller indexes were assigned using the Maud software package.

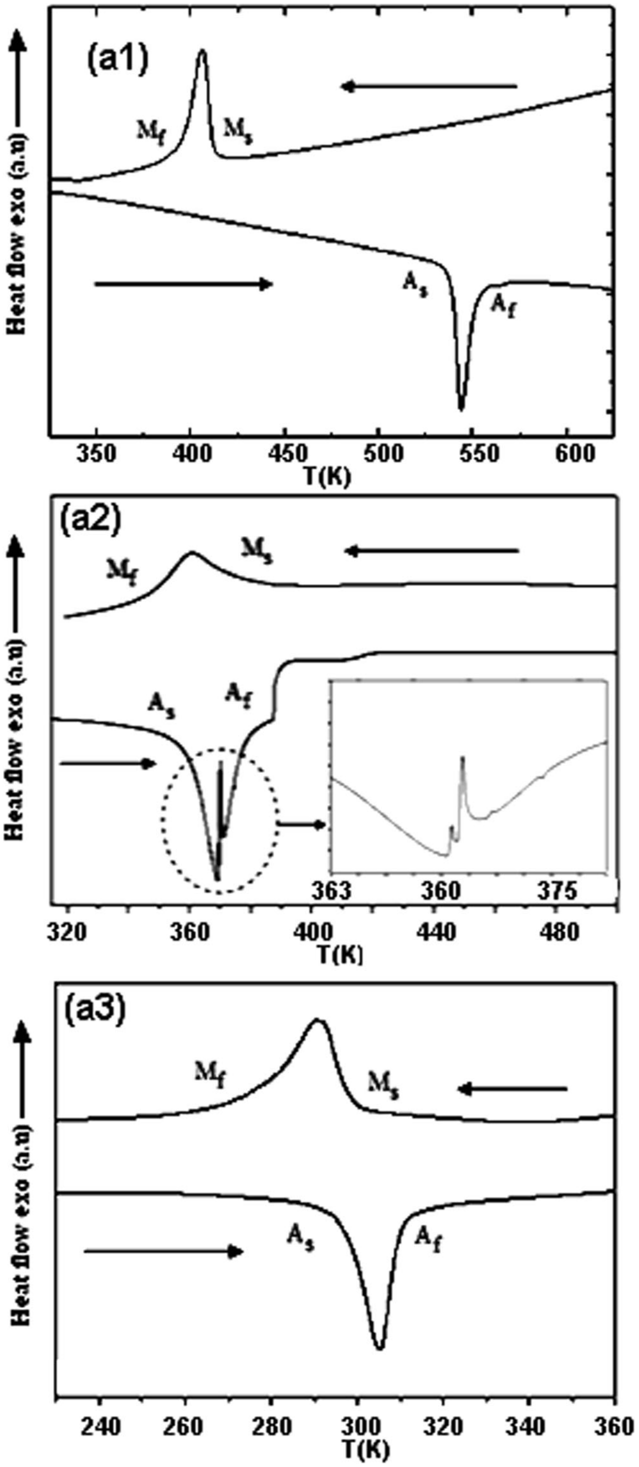

Fig. 5 DSC cyclic scan for the alloys: **a** $Mn_{50}Ni_{43}Sn_7$, **b** $Mn_{50}Ni_{41.3}Sn_{8.7}$, and **c** $Mn_{50}Ni_{39.5}Sn_{10.5}$ samples at a heating/cooling rate of 10 K/min. *Arrows* indicate heating (*up*: austenite to martensite) and cooling (*down*: martensite to austenite)

The XRD patterns of Sn7 and Sn8.7 ribbons illustrates a martensite phase of monoclinic 14-M structure with lattice parameter $a = 0.4301(3)$ nm, $b = 0.561(4)$ nm, $c = 2.996(7)$ nm, and $\beta = 93.37°$ for Sn7 and $a = 0.4315$ nm, $b = 0.5797$ nm, $c = 3.0245$ nm, and $\beta = 93.84°$ for Sn8.7 ribbons. The inset of Fig. 3 (a1, a2) corresponds to the range of $39° \leq 2\theta \leq 47°$. This may indicate that the temperature of the martensitic transformation (MT) is in the vicinity of room temperature. However, for Sn10.5 ribbons, the UDX patterns indicate that the crystalline austenite phase was the highly ordered cubic Heusler $L2_1$with lattice parameter $a = 0.599(1)$ nm (Fig. 2a3).

In recent work, Wu et al. [20] reported the crystal structure of $Mn_{50}Ni_{42}Sn_8$ alloys at room temperature and they revealed the martensite with a non-modulated body-centered tetragonal structure with lattice parameters $a = b = 0.545$ nm, and $c = 0.697$ nm.

XRD lattice parameters are given in Table 1. The monoclinic phase is the same in Sn7 and Sn8.7 alloys. Nevertheless, the relative peak intensity is different. It is known that Heusler alloys sometimes present texture effects [4]. This effect is easier to be detected in alloys with ribbon shape due to the formation of columnar grains in the rapid solidification process. However, in Sn10.5 ribbons, the peak reflections indexed as (3 1 1), and (3 3 1) confirm the existence of the highly ordered cubic Heusler $L2_1$ structure with lattice parameter $a = 0.599$ nm (Fig. 4c3).

On the basis of the XRD results, it is clear that the DSC scans of Sn7 and Sn8.7 ribbons should be performed by heating from room temperature in order to detect the martensite–austenite transition. While the DSC scan of Sn10.5 alloy could be performed by cooling from room temperature.

Recently, some interesting reports on the physical properties of Mn–Ni–Sn Heusler alloy have been published. Coll et al. [19] found that Mn–Ni–Sn alloys are fully single-phase with a cubic structure austenite phase at room temperature and this thermally transforms into structurally modulated orthorhombic martensite upon cooling.

From XRD diffraction patterns, it is clear that DSC scans of alloys Sn7 and Sn8.7 should be performed by heating from room temperature in order to detect the martensite–austenite transition (Fig. 5a1 and a2). Likewise, DSC scan of alloy Sn10.5 should be performed by cooling from room temperature Fig. 5a3. The characteristic transformation temperatures (martensite start and finish and austenite start and finish temperatures are $M_{s.}$, M_f, A_s, and A_f, respectively) are determined from the DSC curves and are collected in Table 2. Moreover, it can be clearly seen that the small humps of alloys Sn8.7, possibly due to a local inhomogeneous composition beyond the resolution of ED's measurement, emerge in the MT temperature region during cooling in the case of As-spun ribbons, as indicated by arrow in Fig. 5. The same resolution is reported by H. Zeng et al. [21].

The hysteresis is due to the increase of the elastic and surface energies during the martensite formation. Thus, the nucleation of the martensite implies supercooling. The width of the hysteresis, ΔT ($\Delta T = A_s - M_f$), is determined as the difference between the temperatures corresponding to the peak positions. The values obtained upon cooling and heating were about 174.10 and 14 K for Sn7, Sn8.7, and Sn10.5 ribbons, respectively. The start and end of the transformation temperatures have been determined by noting the intersection of a baseline and the tangents to each peak. This clearly indicated the first-order nature of the structural transformation from the austenite to the martensite phase upon cooling and reverse transformation upon heating. In addition, the transformation region can be characterized by the martensite transformation temperature T_0 (the temperature at which the Gibbs energies of martensitic and parent phases are related to the $M_{s.}$ and A_f parameters by the equation: $T_0 = 1/2(M_s + A_f)$ [22]). The values of T_0 were calculated; T_0 values are 482 K, 383.7 K, and 305 K for alloys Sn7, Sn8.7, and Sn10.7, respectively.

The transformation temperatures of shape memory alloys strongly depend on the composition and their values spread in a very wide range. Similar results were found in other NiMn (In, Sn) Heusler alloys [8, 23]. To further characterize this alloy, the average number of valence electrons by atom (e/a) parameter was introduced. The calculated value of e/a is equal to 8.08, 7.97, and 7.87 for Sn7, Sn8.7, and Sn10.7 alloys, respectively.

Structural transition temperatures in Heusler alloys can be altered by changing the composition or by doping [24]. Sanchez-Alorcos et al. [25] have reported the martensitic transition temperature is dependent on the valence electron concentration (e/a ratio).

The dependence of transition temperatures on Sn concentration can be explained in terms of the valence electron

Table 2 Transformation temperatures and thermodynamic parameters: h and c indicates data obtained by heating or cooling DSC scans, respectively

Ribbons	M_s (K)	M_f (K)	A_s (K)	A_f (K)	T_0 (K)	ΔH (J g^{-1})	ΔS(J g^{-1}.k^{-1})	e/a
Sn7	394	374	548	570	482	21.206 (h) 19.484 (c)	0.043 (h) 0.04 (c)	8.08
Sn8.7	380	345	355	387.5	383.7	12.42 (h) 10.8 (c)	0.33 (h) 0.029 (c)	7.97
Sn10.5	300	275	293	310	305	6.63 (h) 7.8 (c)	0.021 (h) 0.026 (c)	7.87

concentration (*e*/*a*). All the transition temperatures decrease with the decrease in the value of the outer electron concentration (*e*/*a*) (with increase in Sn concentration). This behavior of dependence of martensitic transition temperatures on *e*/*a* ratio was observed for Ni–Mn–Z (Z = Ga, Sn, In, and Sb) alloys [16].

In a recent work, from the results of DSC measurements, Jyoti Sharmaa and K.G. Suresh [26] have reported the characteristic temperatures of martensitic transformation which were found to be (M_s = 223 K, M_f = 182 K, A_s = 190 K, and A_f = 227 K) for ternary $Mn_{50}Ni_{40}Sn_{10}$ ribbons. Zhida Han et al. [27] have also determined the transformation temperatures (M_s = 300 K, M_f = 280 K, A_s = 290 K, and A_f = 320 K) for ternary $Mn_{50}Ni_{41}Sn_9$ ribbons.

The entropy and enthalpy changes (ΔS and ΔH, respectively) of the structural transformations are calculated from the baseline calorimetry data [2]. The calculated values of enthalpy (ΔH) and thermal entropy (ΔS) changes obtained from cooling (heating) curve are collected in Table 2. It is to be noted that both the enthalpy and entropy changes decrease with the decrease in *e*/*a* ratio, caused by the increase of Sn concentration. Krenke et al. [2] have previously reported that both ΔS and ΔH increased with the increase of *e*/*a* concentration for Ni–Mn–In and Ni–Mn–Sn ternaries. It has, for instance, been reported that the concentration value of *e*/*a* = 8.292 corresponded to ΔH = 3500 J mol^{-1} and ΔS = 4.6 J mol^{-1} K^{-1}. Recently, Wu et al. [28] reported the enthalpy (ΔH) and entropy (ΔS) changes of the $Mn_{50}Ni_{40}In_{10}$ alloy and they found the values of 9.7 J/g and 25 J K^{-1}kg^{-1}, respectively. Moreover, they found that both the enthalpy and entropy changes increased continuously with increasing of (*e*/*a*) ratio values.

The Sn added instead of $Mn_{50}Ni_{50-x}Sn_x$ has a marked effect on martensitic transition temperatures. In $Mn_{50}Ni_{50-x}Sn_x$ the substitution of Sn by Ni significantly affects M_s and M_f, determined from the results of DSC measurements. It is reported that Sn doping in $Mn_{50}Ni_{50-x}Sn_x$ increases the M_s. The substitution of Sn by Ni changes the value of *e*/*a*, which can be explained in terms of *e*/*a* (*e*/*a* increase → M_s increase).

4 Conclusion

In the present paper, we have investigated the structures and martensitic transformation properties of the $Mn_{50}Ni_{50-x}Sn_x$ (x = 7, Sn8.7, and 10.5) ribbons based on the obtained experimental results and some conclusions may be drawn.

1. The results from calorimetric and X-ray diffraction pattern analysis at room temperature confirmed that MT occurred above room temperature for 7 and Sn8.7 and near room temperature for Sn10.5. Columnar grains and preferential orientation were obtained from morphological analysis.
2. As determined from the analysis of X-ray diffraction patterns at room temperature, alloys with Sn5 and Sn7.5 has a textured monoclinic 14-M martensite structure whereas alloy with Sn10 has an austenite cubic $L2_1$ structure.
3. The austenite to martensite reversible transformation was found in all samples. As expected, M_s increases as increasing *e*/*a* (valence electron by atom). Thus, the *e*/*a* control permits the development of alloys with the desired transformation temperatures. Likewise, the entropy and enthalpy change related to the transformation decreases as decreasing *e*/*a*.

Acknowledgments This study was supported by financial funds from the MAT2013-47231-C2-2-P project. The authors would like to express their gratitude to Xavier Fontrodona Gubau for her XRD support.

References

1. Sunol JJ, Escoda L, Hernando B, Sanchez LIamazares JL, Prida VM (2009) Structural behavior of Ni-Mn-(In, Sn) Heusler melt spun ribbons. J ESOMAT 02031
2. Krenke T, Acet M, Wassermann EF, Moya X, Manosa L, Planes A (2005) Martensitic transitions and the nature of ferromagnetism in the austenitic and martensitic states of Ni-Mn-Sn alloys. J Phys Rev B 72:014412
3. Fukushima K, Sano K, Kanomata T, Nishihara H, Furutani Y, Shishido T, et al. (2009) Phase diagram of Fe-substituted Ni–Mn–Sn shape memory alloys. J Scripta Mater 61:813–816
4. Sanchez-Llamazares JL, Sanchez T, Santos JD, Pérez MJ, Sanchez ML, Hernando B, et al. (2008) Martensitic phase transformation in rapidly solidified $Mn_{50}Ni_{40}In_{10}$ alloy ribbons. J Appl Phys Lett 92: 012513
5. Xuan HC, Xie KX, Wang DH, Han ZD, Zhang CL, Gu BX, et al. (2008) Effect of annealing on the martensitic transformation and magnetocaloric effect in $Ni_{44.1}Mn_{44.2}Sn_{11.7}$ ribbons. Appl Phys Lett 92:242506
6. Anantharman TR, Suryanarayana C (1987) Rapidly solidified metals: a technological overview; Trans Tech Publications, Aedermannsdorf Switzerland 260
7. Hernando B, Sanchez Llamazares JL, Prida VM, Baldomir D, Serantes D, Ilyn M, et al. (2009) Magnetocaloric effect in preferentially textured $Mn_{50}Ni_{40}In_{10}$ melt spun ribbons. J Appl Phys Lett 94:222502
8. Santos JD, Sanchez T, Alvarez P, Sanchez ML, Sanchez Llamazares JL, Hernando B (2008) Microstructure and magnetic properties of $Ni_{50}Mn_{37}Sn_{13}$ Heusler alloy ribbons. J Appl Phys 07B326:103
9. Manosa L, Moya X, Planes A, Gutfleisch O, Lyubina J, Barrio M, Tamarit JL, Aksoy S, Krenke T, Acet M (2008) Effects of hydrostatic pressure on the magnetism and martensitic transition of Ni-Mn-In magnetic superelastic alloys. J Appl Phys Lett 92:012515
10. Wang DH, Zhang CL, Han ZD, Xuan HC, Gu BX, Du YW (2008) Large magnetic entropy changes and magnetoresistance in $Ni_{45}Mn_{42}Cr_2Sn_{11}$ alloy. J Appl Phys 103:033901
11. Krenke T, Duman E, Acet M, Moya X, Manosa L, Planes A (2007) Effect of Co and Fe on the inverse magnetocaloric properties of Ni-Mn-Sn. J Appl Phys 102:033903
12. Bachaga T, Daly R, Sunol JJ, Saurina J, Escoda L, Legarreta LG, Hernando B, Khitouni M (2015) Effects of Co additions on the

martensitic transformation and magnetic properties of Ni–Mn–Sn shape memoryalloys. J Supercond Nov Magn 28:3087–3092
13. Wang DH, Zhang CL, Xian HC, Han ZD, Zhang JR, Tang SL, Gu BX, Du YW (2007) The study of low-field positive and negative magnetic entropy changes in $Ni_{43}Mn_{46-x}Cu_xSn_{11}$ alloys. J Appl Phys 102:013909
14. Moya X, Manosa L, Planes A, Krenke T, Acet M, Wassermann EF (2006) Lattice dynamics of Ni–Mn–Al Heusler alloys. J Materials science and engineering: A 481-482:227–230
15. Yuhasz WM, Schlagel DL, Xing Q, McCallum RW, Lograsso TA (2010) Metastability of ferromagnetic Ni–Mn–Sn Heusler alloys. J Alloys and Compounds 492:681–684
16. Krenke T, Moya X, Aksoy S, Acet M, Entel P, Manosa L, et al. (2007) Electronic aspects of the martensitic transition in Ni–Mn based Heusler alloys. J Magn Magn Mater 310:2788–2789
17. Bachaga T, Daly R, Khitouni M, Escoda L, Saurina J, Suñol JJ (2015) Thermal and structural analysis of $Mn_{49.3}Ni_{43.7}Sn_{7.0}$ Heusler alloy ribbons. Entropy 17:646–657
18. Lutterotti L, MAUD CPD Newsletter, IUCr (2000) 24
19. Coll R, Escoda L, Saurina J, Sanchez-Llamazares JL, Hernando B, Sunol JJ (2010) Martensitic transformation in Mn–Ni–Sn Heusler alloys. J Therm Anal Calorim 99:905–909
20. Wu Z, Liu Z, Yang H, Liu Y, Wu G (2011) Martensitic and magnetic transformation behaviours in $Mn_{50}Ni_{42-x}Sn_8Co_x$ polycrystalline alloys. J Phys D Appl Phys 44:385403
21. Zeng H, Wu D, Xue S, Frenzel J, Eggeler G, Zhai Q (2011) Martensitic transformation in rapidly solidified Heusler Ni $_{49}Mn_{39}Sn_{12}$ ribbons. J Acta Materialia 59:5692–5699
22. Kaufman L, Hullert M (1992) Thermodynamics of martensite transformation. In: Olson GB, Owen WS (eds) Martensite, ASM International Cambridge, pp. 41–58
23. Hernando B, Sanchez-Llamazares JL, Santos JD, Escoda L, Sunol JJ, Varga R, et al. (2008) Thermal and magnetic field-induced martensite-austenite transition in $Ni_{50.3}Mn3_{5.3}Sn_{14.4}$ ribbons. J Appl Phys Lett 92:042504
24. Planes A, Manosa L, Acet M (2009) Magnetocaloric effect and its relation to shape-memory properties in ferromagnetic Heusler alloys. J Phys Condens Matter 21:233201
25. Sanchez-Alarcos V, Recarte V, Perez-Landazabal JI, Gomez-Polo C, Rodriguez-Velamazan JA (2012) Role of magnetism on the martensitic transformation in Ni–Mn-based magnetic shape memory alloys. J Acta Materialia 60:459–468
26. Sharmaa J, Suresh KG (2015) Investigation of multifunctional properties of $Mn_{50}Ni_{40-x}Co_xSn_{10}$ (x = 0-6) Heusler alloys. J Alloys Compd 620:329–336
27. Han Z, Chen X, Zhang Y, Chen J, Qian B, Jiang X, Wang D, Du Y (2012) Martensitic transformation and magnetocaloric effect in Mn–Ni–Nb–Sn shape memory alloys: the effect of 4d transition-metal doping. J alloys and compounds 515:114–118
28. Wu Z, Liu Z, Yang H, Liu Y, Wu G (2011) Effect of Co addition on martensitic phase transformation and magnetic properties of $Mn_{50}Ni_{40-x}In_{10}Co_x$ polycrystalline alloys. J Intermetallics 19: 1839–1848